Journal of Solid State Chemistry **146,** 538–545 (1999)
Article ID jssc.1999.8428, available online at http://www.idealibrary.com on IDEAL®

LETTER TO THE EDITOR

Hybrid Framework Iron(II) Phosphate-Oxalates

Amitava Choudhury,*,† Srinivasan Natarajan,* and C. N. R. Rao*,†,[1]

*Chemistry and Physics of Materials Unit, Jawaharlal Nehru Centre for Advanced Scientific Research, Jakkur P.O., Bangalore 560 064, India; and †Solid State and Structural Chemistry Unit, Indian Institute of Science, Bangalore 560 012, India

Communicated by H.-C. zur Loye April 6, 1999; accepted June 8, 1999

Two inorganic–organic hybrid framework iron phosphate–oxalates, I, $[N_2C_4H_{12}]_{0.5}[Fe_2(HPO_4)(C_2O_4)_{1.5}]$ and II, $[Fe_2(OH_2)PO_4(C_2O_4)_{0.5}]$, have been synthesized by hydrothermal means and the structures determined by X-ray crystallography. Crystal Data: compound I, monoclinic, spacegroup = $P2_1/c$ (No. 14), $a = 7.569(2)$ Å, $b = 7.821(2)$ Å, $c = 18.033(4)$ Å, $\beta = 98.8(1)^\circ$, $V = 1055.0(4)$ Å^3, $Z = 4$, $M = 382.8$, $D_{calc} = 2.41$ g cm^{-3}, Mo$K\alpha$, $R_F = 0.02$; compound II, monoclinic, spacegroup = $P2_1/c$ (No. 14), $a = 10.240(1)$ $b = 6.375(3)$ Å, $c = 9.955(1)$ Å, $\beta = 117.3(1)^\circ$, $V = 577.4(1)$ Å^3, $Z = 4$, $M = 268.7$, $D_{calc} = 3.09$ g cm^{-3}, Mo$K\alpha$, $R_F = 0.03$. These materials contain a high proportion of three-coordinated oxygens and $[Fe_2O_9]$ dimeric units, besides other interesting structural features. The connectivity of Fe_2O_9 is entirely different in the two materials resulting in the formation of a continuous chain of Fe–O–Fe in II. The phosphate–oxalate containing the amine, I, forms well-defined channels. Magnetic susceptibility measurements show Fe^{II} to be in the high-spin state ($t_{2g}^4e_g^2$) in II, and in the intermediate-spin state ($t_{2g}^5e_g^1$) in I.

INTRODUCTION

The field of open-framework inorganic materials has emerged to become an active area of research in the last decade. Although the primary motivation for the study has been to design materials comparable to aluminosilicate zeolitic structures with catalytic and other surface properties, the discovery of new materials with novel structural features has assumed equal importance. Among the open-framework materials, metal phosphates occupy a prime position. In particular several open-framework phosphates of Zn, Al, and other metals have been prepared and characterized (1). A few transition metal phosphates with open-framework structures have also been reported, especially those involving Co and Fe (2–6). During the course of our investigations of open-framework transition metal phosphates, we have discovered two phosphate–oxalates of iron, which constitute an interesting family of framework structures. One of the phosphate–oxalates contains the structure-directing amine (**I**) in the channels whereas the other (**II**) is devoid of the amine molecule.

EXPERIMENTAL

The iron oxalate–phosphates, **I** and **II**, were prepared under mild hydro/solvothermal conditions starting from a mixture containing piperazine (PIP) (**I**) or 1,3-diaminopropane (DAP) (**II**) respectively, as the structure-directing agent. For **I**, iron(II) oxalate, phosphoric acid (85 wt%, Aldrich), PIP and water in the ratio FeC_2O_4 : 1.89 H_3PO_4 : PIP : 200 H_2O were taken in the starting mixture. For **II**, iron oxalate, phosphoric acid, DAP and water were mixed in the ratio FeC_2O_4 : H_3PO_4 : PIP : 200 H_2O. The starting mixtures were stirred to attain homogeneity and then sealed in PTFE-lined stainless steel autoclaves (Parr, USA). The initial pH of the mixture for **I** was 2.5 and for **II** 3.5. The sealed pressure vessels were heated at 150°C for 72 h for **I** and for **II** at 150°C for 64 h followed by heating at 170°C for a further period of 48 h. The reaction led to the formation of large quantities of transparent light yellow rod-like (**I**) and plate-like (**II**) crystals along with a small quantity of white powder. The total yield of the products is 70% (**I**) and 40% (**II**) respectively. The crystals were easily separated using sonification procedure in aqueous medium and used for all further studies. Initial characterization was carried out using powder X-ray diffraction (XRD) and thermogravimetric analysis (TGA). Powder XRD patterns on the powdered crystals indicated that the products were new; the pattern is entirely consistent with the structure determined by single crystal X-ray diffraction. Magnetic suceptibility measurements on **I** and **II** were carried out in the 30–300 K range using a Lewis coil magnetometer.

[1]To whom correspondence should be addressed. E-mail: cnrrao@jncasr.ac.in.

0022-4596/99 $30.00

Single crystal structure determination by X-ray diffraction was performed on a Siemens Smart-CCD diffractometer equipped with a normal focus, 2.4 kW sealed tube X-ray source (Mo$K\alpha$ radiation, $\lambda = 0.71073$ Å) operating at 50 kV and 40 mA. A hemisphere of intensity data was collected at room temperature in 1321 frames with ω scans (width of 0.30° and exposure time of 10 s per frame). Pertinent details for the structure determination are listed in Table 1. The structure was solved by direct methods using SHELXS-86 (7) and difference Fourier syntheses. An empirical absorption correction based on symmetry equivalent reflections was applied using SADABS program (8). Other effects such as absorption by the glass fiber were simultaneously corrected. All the hydrogen positions of both the framework and the amine molecules were initially found in the difference Fourier maps and for the final refinement the hydrogen atoms were placed geometrically and held in the riding mode. The last cycles of refinement included atomic positions, anisotropic thermal parameters for all the nonhydrogen atoms, and isotropic thermal parameters for all the hydrogen atoms. Full-matrix least-squares structure refinement against $|F^2|$ was carried out using SHELXTL-PLUS (9) package of programs. Details of final refinements are presented in Table 1. The final factional atomic coordinates and selected bond distances and angles for compound **I** are presented in Tables 2 and 3 and for **II** in Tables 4 and 5, respectively.

TABLE 1

Crystal Data and Structure Refinement Parameters for I $[N_2C_4H_{12}]_{0.5}[Fe_2(HPO_4)(C_2O_4)_{1.5}]$ and II $[Fe_2(OH_2)PO_4(C_2O_4)_{0.5}]$

	I	II
Empirical formula	$Fe_2PO_{10}C_5N_1H_6$	$Fe_2PO_7C_1H_2$
Crystal system	Monoclinic	Monoclinic
Space group	$P2_1/c$	$P2_1/c$
Crystal size (mm)	$0.12 \times 0.14 \times 0.24$	$0.12 \times 0.12 \times 0.16$
a (Å)	7.569(2)	10.240(1)
b (Å)	7.821(2)	6.375(3)
c (Å)	18.033(4)	9.955(1)
α (°)	90.0	90.0
β (°)	98.8(1)	117.3(1)
γ (°)	90.0	90.0
Volume (Å^3)	1055.0(4)	577.4(1)
Z	4	4
Formula mass	382.8	268.7
ρ_{calc} (gcm^{-3})	2.41	3.09
λ (Mo$K\alpha$) Å	0.71073	0.71073
μ (mm^{-1})	2.95	5.28
θ range (°)	2.29–23.3	2.24–23.24
Total data collected	4254	2280
Index ranges	$-8 \le h \le 8$, $-8 \le k \le 8$, $-18 \le l \le 20$	$-11 \le h \le 8$, $-7 \le k \le 7$, $-8 \le l \le 11$
Unique data	1514	824
Observed data ($\sigma > 2\sigma(I)$)	1371	759
Refinement method	Full-matrix least-squares on $[F^2]$	Full-matrix least-squares on $[F^2]$
R indices $[I > 2\sigma(I)]$	$R_1 = 0.021$; $wR_2 = 0.062$	$R_1 = 0.027$; $wR_2 = 0.066$
R indices (all data)	$R_1 = 0.026$; $wR_2 = 0.063$	$R_1 = 0.034$; $wR_2 = 0.096$
Goodness of fit (S)	1.17	1.37
No. of variables	173	109
Largest difference Map peak and hole eÅ^{-3}	0.423 and −0.466	1.034 and −0.962

RESULTS AND DISCUSSION

Two new iron(II) phosphate–oxalates, **I** $[N_2C_4H_{12}]_{0.5}[Fe_2(HPO_4)(C_2O_4)_{1,5}]$ and **II** $[Fe_2(OH_2)PO_4(C_2O_4)_{0.5}]$, have been obtained as good quality single crystals by hydrothermal synthesis. The asymmetric unit of **I** $[C_4N_2H_{12}]_{0.5}[Fe_2(HPO_4)(C_2O_4)_{1.5}]$ consists of 19 nonhydrogen atoms (Fig. 1a). The structure comprises a network of FeO_6 octahedra, FeO_5 trigonal pyramids, PO_4 tetrahedra, and the oxalate groups. The connectivity between these building moieties gives rise to a three-dimensional anionic framework with the formula $[Fe_2(HPO_4)(C_2O_4)_{1.5}]$. Change compensation is achieved by the incorporation of the protonated piperazinium molecule: there are $0.5[C_4N_2H_{12}]$ molecule per framework formula. The FeO_6 octahedra [Fe(1)] and FeO_5 trigonal pyramid [Fe(2)] share their edges forming a new type of dimeric unit $[Fe_2O_9]$. The dimers are linked to each other via the phosphate, with the oxalate units forming the framework structure (Fig. 2).

Along the a axis, the framework structure of **I** is built up of a chain of edge-sharing four-membered rings made by the $[Fe_2O_9]$ dimers and the phosphate groups, connected to each other via the oxalate bridges forming a sheet-like architecture (Fig. 3a). The individual sheets are connected via another oxalate unit completing the framework architecture (Fig. 3b). The connectivity between the chains and the oxalates creates an eight-membered (four (Fe_2O_6) dimers, two phosphates, and two oxalate units) one-dimensional channel of 7.1×5.4 Å (longest atom–atom contact distances not including the van der Waals radii). The protonated piperazinium cation resides in the middle of the channel (Figs. 3a and 3b). Along the b axis, the structure can be visualized as constructed entirely by oxalate groups, the $[Fe_2O_9]$ dimers forming a sheet, which are connected by the $[HPO_4]$ groups. The connectivity between these units also creates eight-membered one-dimensional channels of 5.9×5.7 Å and also gives rise to a narrow elliptical channel formed by four $[Fe_2O_9]$ dimers, two oxalate, and four phosphate groups (Fig. 4). The various bond distances (Fe–O, P–O, and C–O) as well as bond angles (O–Fe–O, O–P–O, and O–C–O) are as expected for this type of bonding (Table 3). Bond valence sum calculations (10) indicate that one of the oxygens bound to P [(O(10)] is a terminal hydroxyl group.

TABLE 2
Atomic Coordinations [$\times 10^4$] and Equivalent Isotropic Displacement Parameters [$Å^2 \times 10^3$] for I, $[N_2C_4H_{12}]_{0.5}[Fe_2(HPO_4)(C_2O_4)_{1.5}]$

Atom	x	y	z	U(eq)[a]
Fe(1)	3659(1)	565(1)	6352(1)	14(1)
Fe(2)	7122(1)	− 2020(1)	6901(1)	16(1)
P(1)	4460(1)	− 829(1)	8091(1)	12(1)
O(1)	4220(3)	3065(2)	6399(1)	18(1)
O(2)	1951(3)	− 1516(3)	6169(1)	22(1)
O(3)	5847(3)	− 535(2)	5926(1)	19(1)
O(4)	5059(3)	− 661(2)	7322(1)	18(1)
O(5)	2982(3)	977(3)	5124(1)	23(1)
O(6)	1391(3)	1299(2)	6974(1)	20(1)
O(7)	5788(3)	− 4112(2)	6560(1)	20(1)
O(8)	9434(3)	− 2642(3)	6428(1)	19(1)
O(9)	8818(3)	119(3)	7212(1)	20(1)
O(10)	2549(3)	− 1693(3)	7997(1)	22(1)
C(12)	10577(4)	− 1475(4)	6469(2)	16(1)
C(11)	10242(4)	132(4)	6935(2)	16(1)
C(10)	5838(4)	− 444(3)	5222(2)	15(1)
N(1)	1138(4)	4682(4)	5684(2)	36(1)
C(2)	− 452(5)	3603(5)	5461(2)	38(1)
C(1)	1873(5)	5383(5)	5031(2)	38(1)

[a] U(eq) is defined as one third of the trace of the orthogonalized U_{ij} tensor.

The asymmetric unit of **II**, $[Fe_2(OH_2)PO_4(C_2O_4)_{0.5}]$, consists of 11 nonhydrogen atoms (Fig. 1b). The structure is made from a network of FeO_6 octahedra, FeO_5 trigonal pyramid, PO_4 tetrahedra, and the oxalate groups. The connectivity between these building results in a three-dimensional neutral framework with the formula $[Fe_2(OH_2)(PO_4)(C_2O_4)_{0.5}]$. Of the 7 oxygen atoms of the asymmetric

TABLE 3
Selected Bond Distances and Angles in I, $[N_2C_4H_{12}]_{0.5}[Fe_2(HPO_4)(C_2O_4)_{1.5}]$

Moiety	Distance (Å)	Moiety	Angle (°)
Fe(1)–O(1)	1.999(2)	O(3)–Fe(1)–O(5)	76.8(1)
Fe(1)–O(2)	2.073(2)	O(4)–Fe(1)–O(5)	153.6(1)
Fe(1)–O(3)	2.111(2)	O(1)–Fe(1)–O(6)	84.4(1)
Fe(1)–O(4)	2.130(2)	O(2)–Fe(1)–O(6)	77.1(1)
Fe(1)–O(5)	2.218(2)	O(3)–Fe(1)–O(6)	168.4(1)
Fe(1)–O(6)	2.265(2)	O(4)–Fe(1)–O(6)	91.5(1)
Fe(2)–O(7)	1.971(2)	O(5)–Fe(1)–O(6)	112.4(1)
Fe(2)–O(8)	2.117(2)	O(7)–Fe(2)–O(8)	95.7(1)
Fe(2)–O(9)	2.131(2)	O(7)–Fe(2)–O(4)	99.0(1)
Fe(2)–O(3)	2.203(2)	O(8)–Fe(2)–O(4)	163.2(1)
Fe(2)–O(4)	2.123(2)	O(7)–Fe(1)–O(9)	173.3(1)
		O(8)–Fe(2)–O(9)	77.6(1)
Moiety	Angle (°)	O(4)–Fe(2)–O(9)	87.7(1)
		O(7)–Fe(2)–O(3)	92.7(1)
O(1)–Fe(1)–O(2)	153.8(1)	O(4)–Fe(2)–O(3)	76.4(1)
O(1)–Fe(1)–O(3)	103.9(1)	O(8)–Fe(2)–O(3)	95.1(1)
O(2)–Fe(1)–O(3)	97.3(1)	O(9)–Fe(2)–O(3)	88.2(1)
O(1)–Fe(1)–O(4)	109.2(1)	Fe(1)–O(3)–Fe(2)	101.4(1)
O(2)–Fe(1)–O(4)	89.8(1)	Fe(2)–O(4)–Fe(1)	103.4(1)
O(3)–Fe(1)–O(4)	78.2(1)		
O(1)–Fe(1)–O(5)	85.2(1)		
O(2)–Fe(1)–O(5)	85.0(1)		

TABLE 4
Atomic Coordinations [$\times 10^4$] and Equivalent Isotropic Displacement Parameters [$Å^2 \times 10^3$] for II, $[Fe_2(OH_2)PO_4(C_2O_4)_{0.5}]$

Atom	x	y	z	U(eq)[a]
Fe(1)	6217(1)	1424(1)	4774(1)	11(1)
Fe(2)	7333(1)	5194(1)	7366(1)	14(1)
P(1)	6050(1)	6509(2)	3980(1)	9(1)
O(1)	6601(4)	4612(5)	5096(4)	12(1)
O(2)	5414(4)	949(5)	2396(4)	12(1)
O(3)	8280(4)	939(6)	4639(4)	14(1)
O(4)	7793(5)	1445(6)	7206(4)	16(1)
O(5)	4190(4)	1709(5)	5100(4)	13(1)
O(6)	7187(4)	7964(5)	8447(4)	13(1)
O(7)	9656(4)	5799(6)	8176(4)	19(1)
C(1)	9617(6)	505(8)	5437(6)	13(1)

[a] U(eq) is defined as one third of the trace of the orthogonalized U_{ij} tensor.

TABLE 5
Selected Bond Distances and Angles in II, $[Fe_2(OH_2)PO_4(C_2O_4)_{0.5}]$

Moiety	Distance (Å)	Moiety	Distance (Å)
Fe(1)–O(1)	2.067(3)	Fe(2)–O(1)[b]	2.062(3)
Fe(1)–O(2)	2.141(3)	Fe(2)–O(2)[b]	2.109(4)
Fe(1)–O(3)	2.199(3)	Fe(2)–O(3)	2.138(3)
Fe(1)–O(4)	2.209(4)	Fe(2)–O(6)	2.108(3)
Fe(1)–O(5)	2.250(4)	Fe(2)–O(7)	2.167(4)
Fe(1)–O(5)[a]	2.056(3)		
Moiety	Angle (°)	Moiety	Angle (°)
O(5)[a]–Fe(1)–O(1)	167.2(1)	O(1)–Fe(2)–O(6)	129.4(1)
O(5)[a]–Fe(1)–O(2)	86.8(1)	O(1)–Fe(2)–O(2)[b]	94.6(1)
O(1)–Fe(1)–O(2)	105.1(1)	O(6)–Fe(2)–O(2)[b]	89.9(1)
O(5)[a]–Fe(1)–O(3)	95.4(1)	O(1)–Fe(2)–O(3)[b]	149.3(1)
O(1)–Fe(1)–O(3)	91.6(1)	O(6)–Fe(2)–O(3)[b]	81.2(1)
O(2)–Fe(1)–O(3)	78.7(1)	O(2)[b]–Fe(2)–O(3)[b]	80.9(1)
O(5)[a]–Fe(1)–O(4)	90.3(1)	O(1)–Fe(2)–O(7)	103.0(2)
O(1)–Fe(1)–O(4)	80.4(1)	O(6)–Fe(2)–O(7)	89.1(1)
O(2)–Fe(1)–O(4)	158.3(2)	O(2)[b]–Fe(2)–O(7)	158.0(1)
O(3)–Fe(1)–O(4)	80.1(1)	O(3)[b]–Fe(2)–O(7)	77.2(1)
O(5)[a]–Fe(1)–O(5)	81.0(1)	Fe(2)–O(1)–Fe(1)	107.1(2)
O(1)–Fe(1)–O(5)	91.2(1)	Fe(2)[c]–O(2)–Fe(1)	100.2(1)
O(2)–Fe(1)–O(5)	105.0(1)	Fe(2)[c]–O(3)–Fe(1)	97.5(1)
O(3)–Fe(1)–O(5)	174.6(1)	Fe(1)[a]–O(5)–Fe(1)	99.0(2)
O(4)–Fe(1)–O(5)	95.7(1)		

[a] $-x+1, -y, -z+1$.
[b] $x, -y+1/2, z+1/2$.
[c] $x, -y-1/2, -z+3/2$.

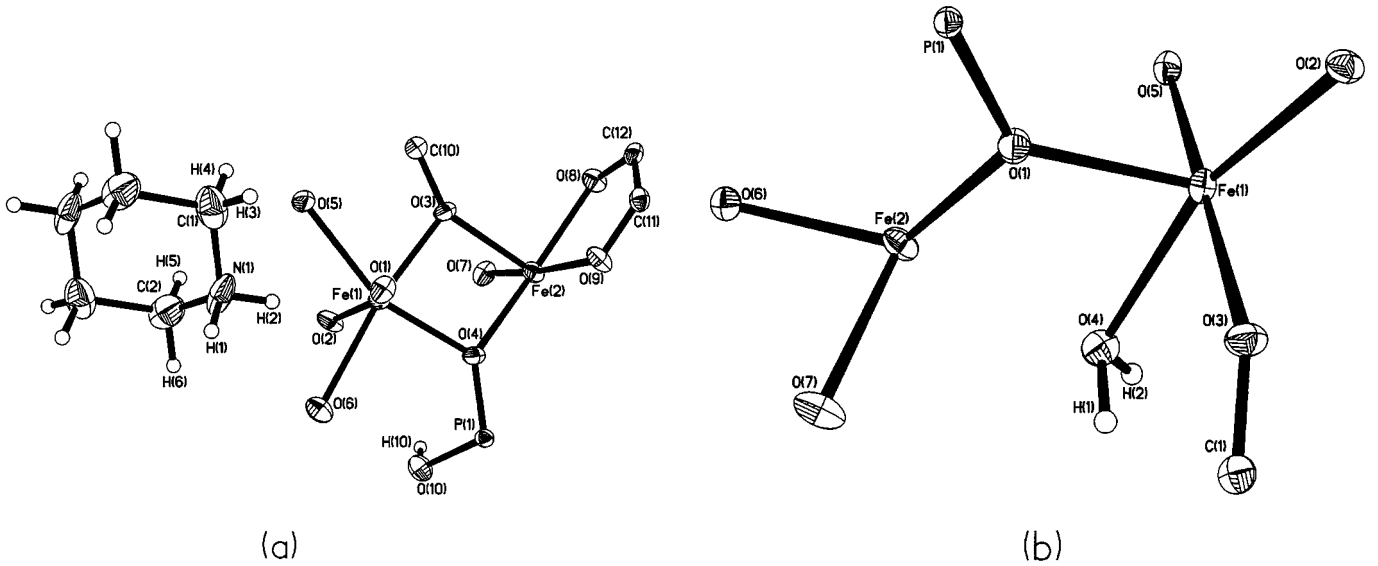

FIG. 1. (a) ORTEP plot of **I**, $[N_2C_4H_{12}]_{0.5}[Fe_2(HPO_4)(C_2O_4)_{1.5}]$. The asymmetric unit is labeled. The thermal ellipsoids are given at 50% probability. (b) ORTEP plot of **II**, $[Fe_2(OH_2)(PO_4)(C_2O_4)_{0.5}]$. The asymmetric unit is labeled. The thermal ellipsoids are given at 50% probability.

unit, 3 oxygens are three coordinated (43%). While O(5) connects two Fe(1) and P atoms, O(1) and O(2) connect Fe(1), Fe(2), and P(1). This type of connectivity makes the structure rather complex.

The FeO_6 octahedra [Fe(1)] and FeO_5 trigonal pyramids [Fe(2)] in **II** share their edges forming $[Fe_2O_9]$ dimers. Four of the dimers are linked via the phosphate groups forming the basic structural building unit which is cross-linked as shown in Fig. 4a. The cross-linked FeO_6 octahedra, FeO_5 trigonal pyramids, and the PO_4 tetrahedra are connected with each other via the oxalate groups (Fig. 5). The presence of a number of three-coordinate oxygens is responsible for the formation of the continuous network of the dimers and hence the polymeric iron–oxygen network (Fig. 4b). The important structural parameters of **II** are listed in Table 5. Bond valence sum calculations (10) indicate that one of the oxygen [O(4)] is a water molecule.

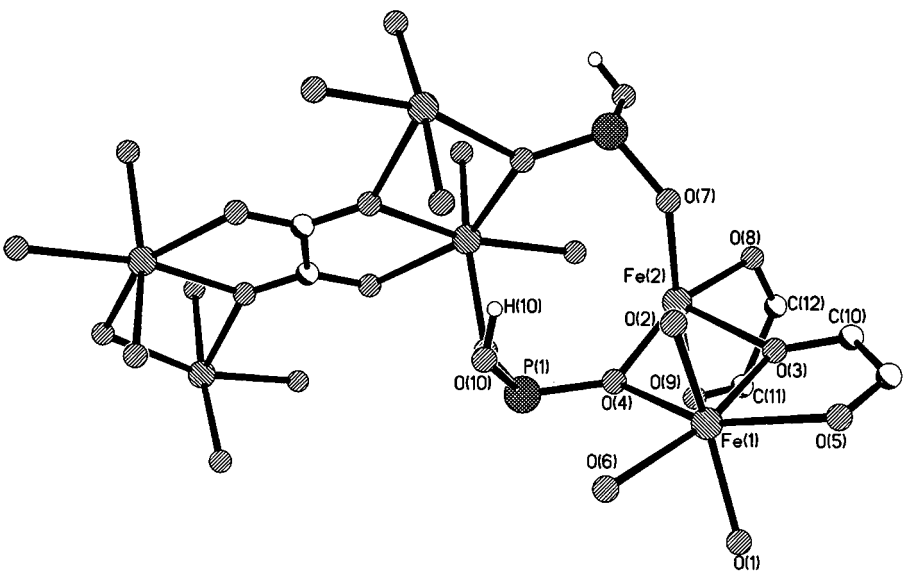

FIG. 2. Structure showing the basic structural building unit in **I**, $[N_2C_4H_{12}]_{0.5}[Fe_2(HPO_4)(C_2O_4)_{1.5}]$. Note that the four-membered ring is formed between the $[Fe_2O_9]$ dimers and the phosphate groups.

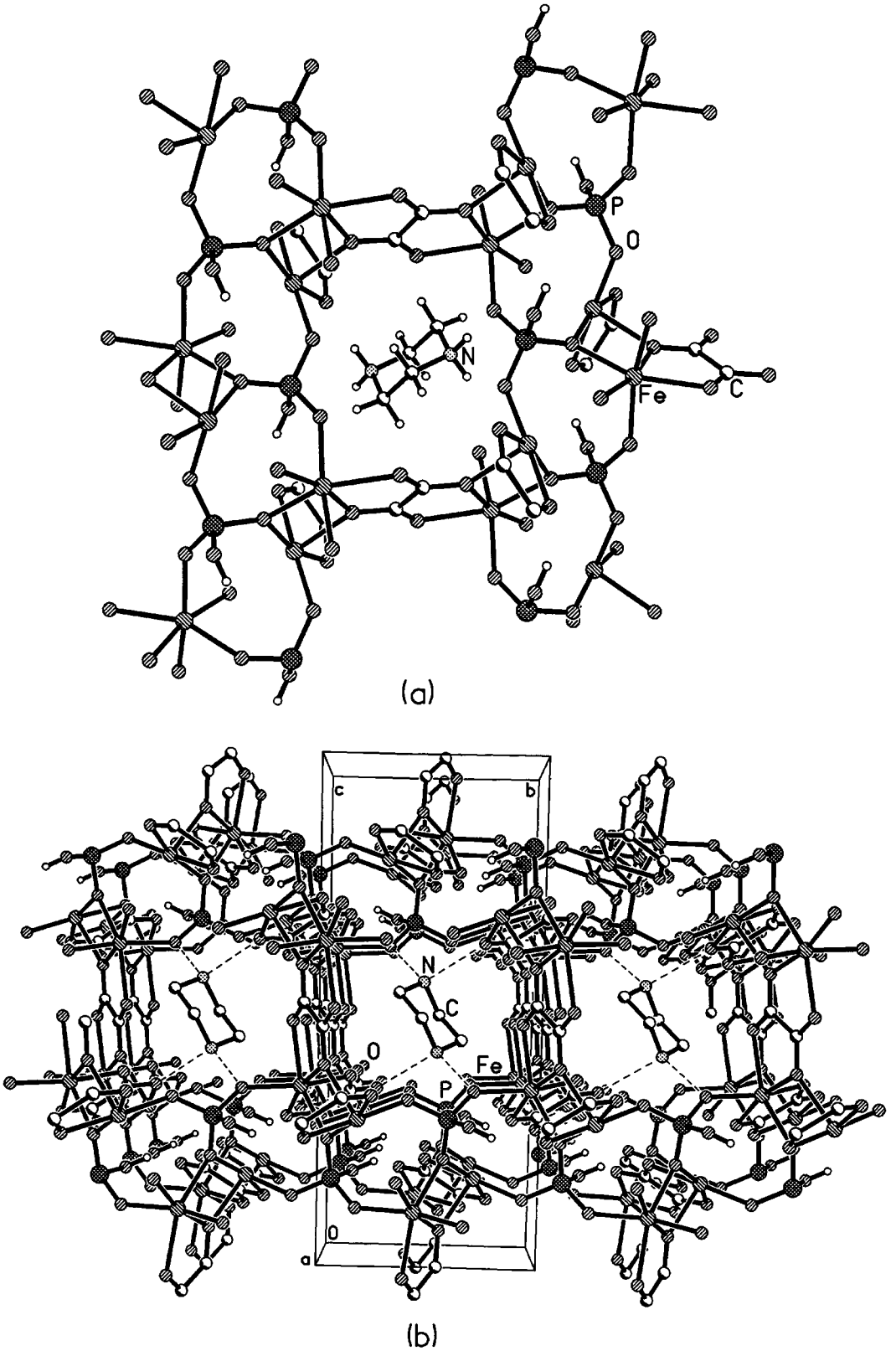

FIG. 3. (a) Structure showing the four-membered chain and the connectivity between the chains via the oxalates leading to the formation of the channels in **I**, $[N_2C_4H_{12}]_{0.5}[Fe_2(HPO_4)(C_2O_4)_{1.5}]$. (b) Structure showing the one-dimensional channels in **I**, $[N_2C_4H_{12}]_{0.5}[Fe_2(HPO_4)(C_2O_4)_{1.5}]$ along [100] direction.

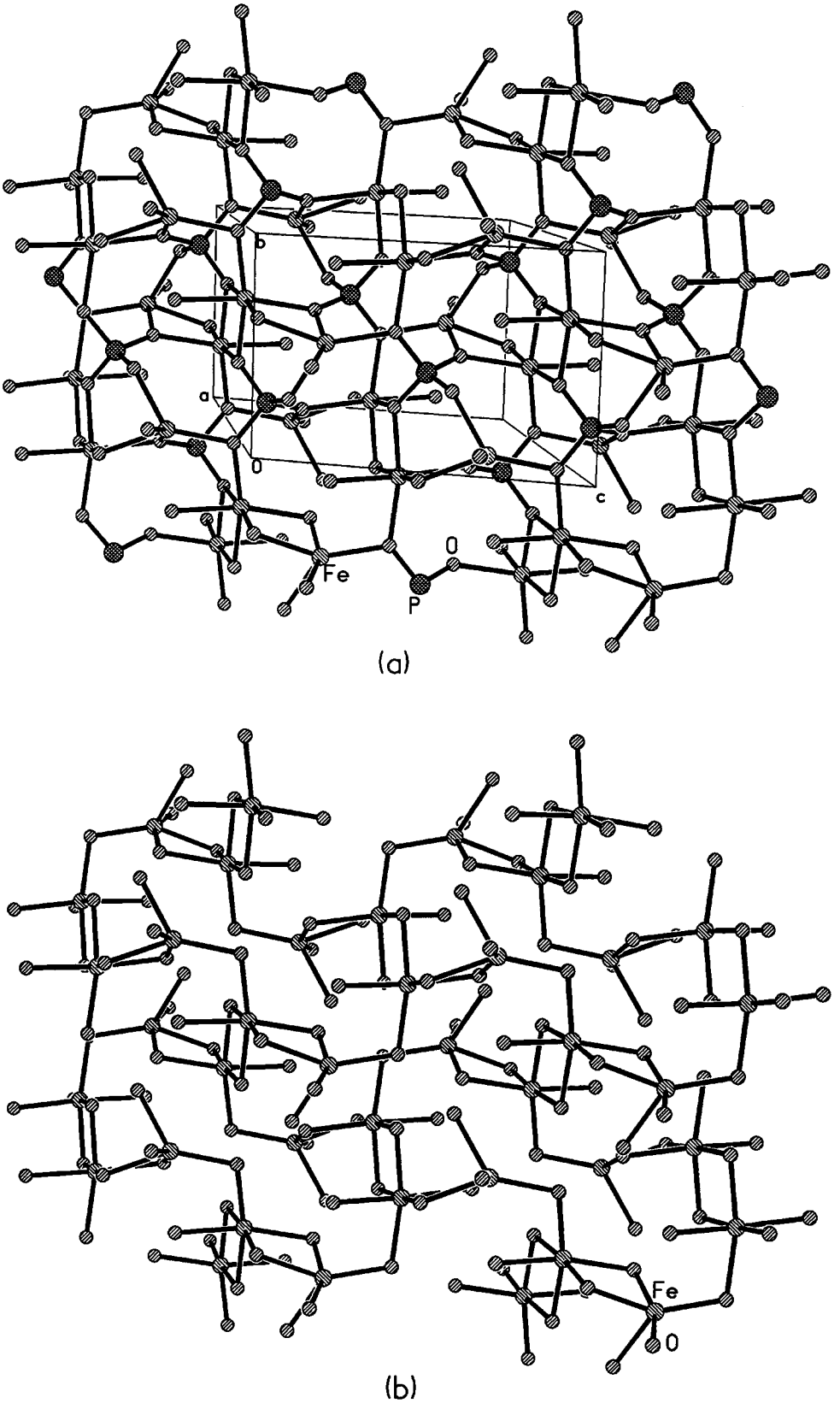

FIG. 4. (a) Structure showing the connectivity between the $[Fe_2O_9]$ dimers and the phosphate tetrahedra in **II**, $[Fe_2(OH_2)PO_4(C_2O_4)_{0.5}]$. (b) Structure showing the Fe subnetwork seen in **II**, $[Fe_2(OH_2)PO_4(C_2O_4)_{0.5}]$. Note that the $[Fe_2O_9]$ dimeric network is continuous.

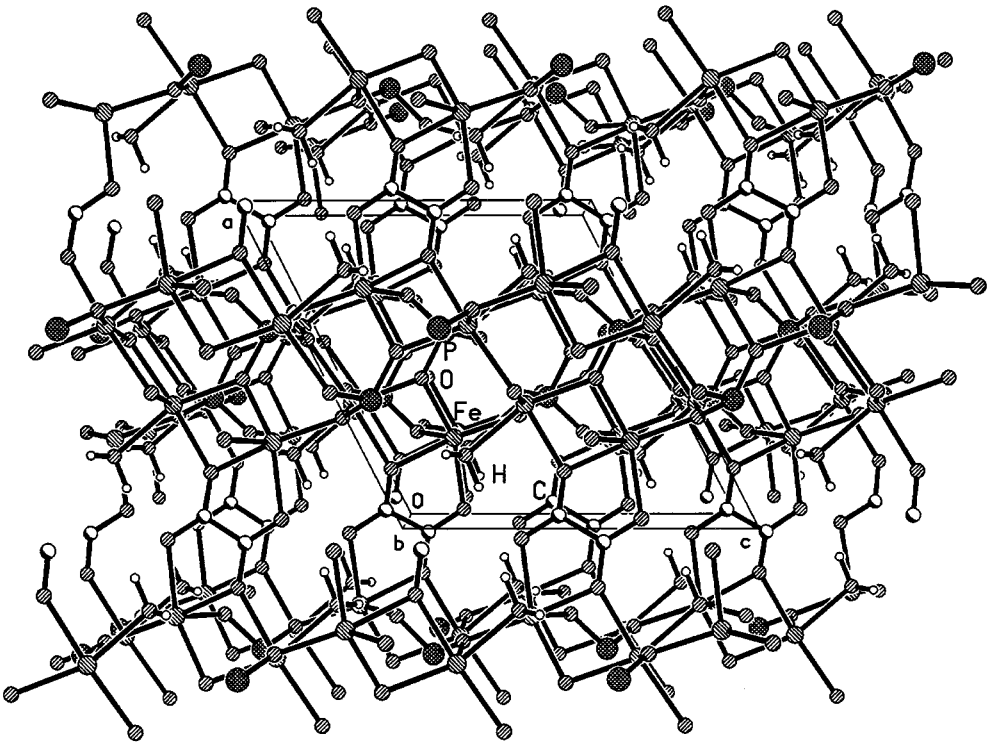

FIG. 5. Structure showing the connectivity between the $[Fe_2O_9]$ dimers, phosphate tetrahedra, and the oxalate units. Note that the oxalate units bridge the layer-type arrangements made by the dimer and the phosphate groups.

The phosphate–oxalates, **I** and **II**, are members of a novel family of hybrid framework structures. Though the synthesis of both these materials was carried out in the presence of structure-directing amines, compound **I** is formed with the amine molecule present as part of the structure, while the amine is absent in **II**. Both **I** and **II** have three-coordinated oxygen atoms as part of the framework. In **I**, two oxygen atoms are three-coordinated whereas in **II** four oxygen atoms are three-coordinated. The presence of a large number of three-coordinated oxygens in **II** leads to a situation wherein all the Fe atoms are connected to one another. The formation of the Fe–O–Fe linkage is accompained by the trigonal coordination of the bridging oxygen atoms, the third coordination being to a P or C atom. The presence of about 40% of the oxygens in the asymmetric unit of **II** (three of the seven framework oxygen atoms) being three-coordinated may have resulted in the formation of a condensed structure in **II**.

The structure-directing amine molecules located within the channels of **I** interact with the framework via multipoint hydrogen bonding. Such multipoint hydrogen bonding is known to be associated with the formation as well as structural stability of the various open-framework materials (11). The hydrogen bond interactions in **I** between the framework and the protonated piperazinium cation are quite strong. The terminal –OH group of the HPO_4 unit participate in intra- as well as interframework hydrogen bonding. The strongest hydrogen bond interactions are: $O(8)\cdots H(1) = 2.023(1)$ Å, $N(1)\text{–}H(1)\cdots O(8) = 162.4(1)^\circ$; $O(1)\cdots H(2) = 1.914(1)$ Å, $N(1)\text{–}H(2)\cdots O(1) = 163.8(1)^\circ$; $O(10)\cdots H(6) = 2.493$ Å, $C(2)\text{–}H(6)\cdots O(10) = 158.5(1)^\circ$. TGA of **I** and **II** were carried out in static air from room temperature to 900°. For **I**, the total mass loss was found to be 41% corresponding to the loss of the amine, oxalate, and –OH groups of the HPO_4 units (calc. 42%) and for **II** the mass loss of 18% corresponds to the loss of water and oxalate unit (calc. 20%). The powder XRD pattern of the decomposed products for **I** corresponded to $Fe_4(P_2O_7)_3$ [JCPDS: 03-0124] and for **II** indicated a poorly crystalline solid that did not correspond with any known condensed iron phosphate.

Magnetic susceptibility measurements for compounds **I** and **II** show interesting differences. In **II**, the temperature-variation of susceptibility follows the Curie–Weiss law with a negative Curie temperature (-35.4 K). The observed magnetic moment (5.15 μ_B) is comparable with the spin-only value (4.89 μ_B) of Fe^{II} in the high-spin state ($t_{2g}^4 e_g^2$). Compound **I**, on the other hand, shows a negative Curie temperature but the overall behavior is different. The magnetic moment of **I** increases from 1.6 μ_B at low temperatures (≤ 150 K) to 3.2 μ_B at high temperatures (≥ 150 K). The high-temperature magnetic moment is characteristic of intermediate spin Fe^{II} ($t_g^5 e_g^1$: calc. 2.82 μ_B).

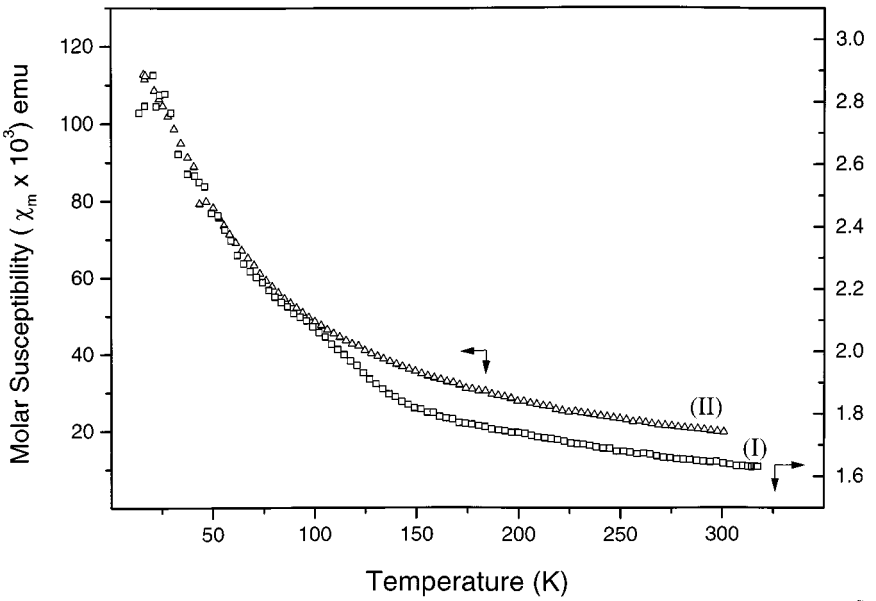

FIG. 6. Temperature variation of the magnetic susceptibility of **I** and **II**.

It is instructive to compare the structural features of **I** with those of the indium phosphate–oxalate reported recently (12). In the indium phosphate–oxalate, networking is between the InO_6 octahedra, PO_4 tetrahedra, and the oxalate units. The structure of **II** containing the iron polymeric network, however, has no known relative in the literature. Since we completed the present study, we noticed a paper on Fe(II) oxalate–phosphate by Lethbridge and Lightfoot (13) which has identical structural formula as **II** and has comparable structural features. The structure reported by Lethbridge and Lightfoot is also made by the networking between the FeO_6, FeO_5, and PO_4 polyhedra forming an iron phosphate sheet that are connected by oxalate bridges forming small cavities wherein the water molecules protrude from iron centers.

CONCLUSIONS

Two iron phosphate–oxalates, constituting a novel class of inorganic–organic hybrid framework solids, have been synthesized under mild hydrothermal/solvothermal conditions. Both the materials have three-dimensional connectivity and comprise Fe_2O_9 dimers. While the Fe_2O_9 dimers are directly connected to one another in **II**, they get connected through phosphate and oxalate units in **I**. In one of the phosphate oxalates, the structure-directing amine is present in well-defined channels formed by the network of the various polyhedra, but the amine is absent in the other phosphate–oxalate. Interestingly, the magnetic properties of **I** and **II** are different. Isolation of two phosphate–oxalates with the Fe in the 2+ state suggests that it would be profitable to explore materials containing Fe in the 3+ oxidation state as well as in the mixed oxidation state.

ACKNOWLEDGMENTS

One of us (A.C.) thanks the Council of Scientific and Industrial Research (CSIR), Government of India for the award of a research fellowship.

REFERENCES

1. W. H. Meier and D. H. Olson, "Atlas of Zeolite Structure Types," Butterworth–Heinemann, London, 1992; J. M. Thomas, *Angew. Chem. Int. Ed. Engl.* **33,** 913 (1994); J. M. Thomas, *Chem. Eur. J.* **3,** 1557 (1997); A. K. Cheetham, G. Ferey, and T. Loiseau, *Angew. Chem. Intl. Ed. Engl.* (1999), in press.
2. J. Chen, R. H. Jones, S. Natarajan, M. B. Hursthouse, and J. M. Thomas, *Angew. Chem. Int. Ed. Engl.* **33,** 639 (1994).
3. J. R. D. DeBord, R. C. Haushalter, and J. Zubieta, *J. Solid State Chem.* **125,** 270 (1996).
4. X. Bu, P. Feng, T. E. Gier, and G. D. Stucky, *J. Solid State Chem.* **136,** 210 (1998) and references therein.
5. P. Feng, X. Bu, and G. D. Stucky, *Nature* **388,** 735 (1997).
6. K.-H. Lii, Y.-F. Huang, V. Zima, C.-Y. Huang, H.-M. Lin, Y.-C. Jiang, F.-L. Liao, and S.-L. Wang, *Chem. Mater.* **10,** 2599 (1998).
7. G. M. Sheldrick, "SHELXS-86 Program for Crystal Structure Determination." University of Göttingen, 1986; *Acta Crystallogr. Sect. A* **35,** 467 (1990).
8. G. M. Sheldrick, "SADABS User Guide." University of Göttingen, 1995.
9. G. M. Sheldrick, "SHELXTL-PLUS Program for Crystal Structure Solution and Refinement." University of Göttingen, 1993.
10. I. D. Brown and D. Altermatt, *Acta Crystallogr. Sect. B* **41,** 244 (1985).
11. M. E. Davis and R. F. Lobo, *Chem. Mater.* **4,** 756 (1992).
12. Y.-F. Huang and K.-H. Lii, *J. Chem. Soc. Dalton Trans.* 4085 (1998).
13. Z. A. D. Lethbridge and P. Lightfoot, *J. Solid State Chem.* **143,** 58 (1999).